Low-Strength Type I Interferon Signaling Promotes CAR T-Cell Treatment Efficacy

Erting Tang[1,#], Yifei Hu[1,2,#], Guoshuai Cao[1], Duy-Thuc Nguyen[1], Nicholas W. Asby[1], Nada S. Aboelella[5], Hanna A. Ruiz[1], Xiaolei Cai[1], Wenbo Zhang[1], Yu Zhao[1], Lishi Xie[3], Xiufen Chen[3], Michael R. Bishop[5,6], Peter A. Riedell[5,6], James L. LaBelle[5], Justin P. Kline[3,4,5,6], Jun Huang[1,3,4,*]

[1]Pritzker School of Molecular Engineering, University of Chicago, Chicago, IL 60637, USA
[2]Pritzker School of Medicine, University of Chicago, Chicago, IL 60637, USA
[3]Committee on Immunology, University of Chicago, Chicago, IL 60637, USA
[4]Committee on Cancer Biology, University of Chicago, Chicago, IL 60637, USA
[5]Section on Hematology/Oncology, Department of Medicine, University of Chicago, Chicago, IL 60637, USA
[6]The David and Etta Jonas Center for Cellular Therapy, University of Chicago, Chicago, IL 60637, USA

[#]These authors contributed equally.
*Corresponding Author:
Jun Huang, PhD
5640 S. Ellis Ave, Chicago, IL, 60637
Email: huangjun@uchicago.edu

RUNNING TITLE
Low-Strength IFN-I Enhances CAR T Cells

DECLARATIONS OF INTERESTS
J.H., Y.H., and E.T. are listed as inventors on a patent related to interferon-enhanced CAR-T cells (US provisional patent application 63/789,043). M.R.B. reports membership on an Advisory Board or Consultancy for Kite/Gilead, Novartis, CRISPR Therapeutics, Autolus Therapeutics, BMS, Incyte, Sana Biotechnology, Iovance Biotherapeutics. He has served on a Speakers Bureau for BMS, Kite/Gilead, Agios, and Incyte. P.A.R. reports Research Support/Funding: BMS, Kite Pharma, Inc./Gilead, MorphoSys, Calibr, Tessa Therapeutics, Fate Therapeutics, Xencor, and Novartis Pharmaceuticals Corporation. Speakers Bureau: Kite Pharma, Inc./Gilead; Consultancy on advisory boards: AbbVie, Novartis Pharmaceuticals Corporation, BMS, Janssen, BeiGene, Karyopharm Therapeutics Inc., Takeda Pharmaceutical Company, Kite Pharma, Inc./Gilead, Sana Biotechnology, Nektar Therapeutics, Nurix Therapeutics, Intellia Therapeutics, and Bayer. Honoraria: Novartis Pharmaceuticals Corporation. J.L.L. reports other grants from AbbVie and the American Cancer Society outside the submitted work. J.P.K. receives research support from Merck, Verastem, and iTeos; has served on a speakers bureau for Kite/Gilead; and has served on advisory boards for Verastem, Seattle Genetics, MorphoSys, and Karyopharm. No disclosures were reported by the other authors.

Abstract: 202 words; Main text: 3937 words; **Figures**: 6; **References**: 52;
Supplementary Tables: 1; **Supplementary Figures**: 9

ABSTRACT

CD19-directed chimeric antigen receptor (CAR) T-cell therapy has significantly advanced the treatment landscape for relapsed/refractory diffuse large B-cell lymphoma (r/r DLBCL). However, up to 60% of patients do not achieve a complete response. To uncover determinants of therapeutic efficacy, we analyzed the infusion products of eight r/r DLBCL patients with distinct clinical responses to axicabtagene ciloleucel using single-cell transcriptomics. Compared to patients who exhibited progressive disease, infusion products of complete responders demonstrated enriched signatures of type I interferon (IFN-I) signaling. Based on these findings, we developed a novel strategy to improve CD19-directed CAR T-cell treatment efficacy by incorporating IFN-I as an enhancer during the *ex vivo* manufacturing process, with IFN-I removal before CAR T-cell infusion to avoid *in vivo* toxicities. For both CD28- and 4-1BB-costimulated second-generation CARs, we found that low-strength IFN-I signaling enhanced CAR T-cell cytotoxicity and treatment efficacy against B-cell lymphoma and leukemia. Our low-strength IFN-I-enhanced CAR T-cell *ex vivo* manufacturing approach leverages an existing FDA-approved pharmacologic agent, circumvents *in vivo* interferon-associated toxicities, and remains fully compatible with current CAR constructs and manufacturing workflows. Together, our results establish IFN-I as a potent and costimulation-independent enhancer of CAR T-cell efficacy and provide a translationally feasible approach to enhance CAR T-cell therapies.

Key Words: chimeric antigen receptor (CAR), type I interferon (IFN-I), axicabtagene ciloleucel (axi-cel), lisocabtagene maraleucel (liso-cel), diffuse large B-cell lymphoma (DLBCL), leukemia

66 **INTRODUCTION**

67

68 Chimeric antigen receptor (CAR) T-cell therapy has advanced the standard-of-care for
69 hematologic malignancies, achieving complete response rates ranging from 39-71% across
70 relapsed/refractory diffuse large B-cell lymphoma (r/r DLBCL)[1], acute lymphoblastic leukemia[2],
71 and multiple myeloma[3,4]. However, the therapy's effectiveness is constrained by significant rates
72 of treatment failure. In r/r DLBCL, only ~40% of patients exhibit a complete response, whereas
73 the remaining ~60% of patients exhibit a partial response, stable disease, or progressive disease,
74 as defined by the International Working Group response criteria.[1] Patients who cannot clear their
75 lymphoma burden have limited therapeutic options and often succumb to their disease.

76 Existing studies have correlated treatment failure with diminished CAR T-cell
77 polyfunctionality[5], increased T-cell exhaustion signatures within CAR T-cell products[6–8], inhibition
78 by CAR Tregs[9], as well as failure of CAR T cells to persist and expand *in vivo*[1,10], among others[11].
79 Given the importance of CAR T-cell-intrinsic factors in determining treatment outcomes, we
80 investigated the infusion products (IP) of CAR T-cell therapy patients with r/r DLBCL using single-
81 cell transcriptomics. We observed that, compared to patients with progressive disease, the IPs of
82 complete responders demonstrated enriched signatures of type I interferon (IFN-I) signaling. This
83 observation was also validated using an independent, published dataset from Maus et al.[12]

84 As potent immunomodulators, IFN-I cytokines have long been of interest for their potential
85 to modulate immunotherapy response rates.[13,14] Upon binding to type I interferon receptors
86 (IFNAR), IFN-I cytokines trigger a phosphorylation cascade that activates transcription factors
87 such as signal transducer and activator of transcription 1 (STAT1), STAT2, and interferon
88 regulatory factor 9 (IRF9).[13] These transcription factors coordinate transcription of interferon-
89 stimulated genes, such as *IRF7*, *MX1*, *ISG15*, *ISG20*, *IFITM1/2/3*, which mediate antiviral
90 immunity and effector functions.[13,15] In $CD8^+$ T cells, IFN-I signaling enhances cytotoxicity[16] and
91 induces central memory differentiation[17], while also controlling T-cell exhaustion[18], inhibitory

92 receptor expression[19], and apoptosis[20,21]. Due to their immunomodulatory effects, clinical
93 formulations of IFN-I cytokines (e.g., Avonex, Intron A, Alferon N) have been approved by the
94 FDA for the treatment of malignancies (e.g., hairy cell leukemia, follicular lymphoma)[22],
95 autoimmune diseases (e.g., multiple sclerosis)[23], and viral infections (e.g., hepatitis B and C)[24].
96 Despite being an attractive FDA-approved cytokine for regulating immune functions in cancer,
97 autoimmunity, and infection, IFN-I has not been utilized to modulate CAR T-cell therapy responses.
98 Given our bioinformatic discoveries and the literature-established roles of T-cell-intrinsic
99 IFN-I signaling in modulating T-cell differentiation and functionality[13], we hypothesize that IFN-I
100 signaling enhances CAR T-cell efficacy during the *ex vivo* manufacturing process. In this study,
101 we detail our discovery and development of IFN-I cytokines as an enhancer to partially address
102 CAR T-cell therapy failure rates. Through *in vitro* functional assays and *in vivo* lymphoma and
103 leukemia xenograft mouse models, we demonstrate proof-of-principle for a better manufacturing
104 method that leverages low-strength, *ex vivo*, and FDA-approved IFN-I cytokines to improve the *in*
105 *vivo* treatment efficacy of CAR T-cell therapy.

106 **MATERIALS AND METHODS**

107

108 *Collection of patient biospecimens*

109 Deidentified patient biospecimens were gathered in accordance with ethical guidelines under the
110 institutional review board at the University of Chicago Medicine. Informed consent was obtained
111 from all patients or their legal guardians prior to sample collection, in compliance with institutional
112 and federal guidelines. All patients received commercially manufactured axi-cel (Yescarta®, Kite
113 Pharma), generated using the same standardized GMP manufacturing protocol at a single
114 external manufacturing facility. Patients were treated at UChicago Medicine between 2019 and
115 2021 and were selected based on the availability of a clearly defined clinical response, as
116 determined by PET/CT imaging at 1 month post-CAR T-cell infusion, as well as the availability of
117 residual infusion product cells for downstream analyses. Residual infusion product cells were
118 collected from each patient's infusion bag, stored in CELLBANKER 1 (Amsbio, 11888), and
119 subsequently cryopreserved in liquid-phase nitrogen for subsequent single-cell sequencing.

120

121 *Single-cell RNA-seq data generation*

122 Cryopreserved biospecimens were thawed and washed with cold FACS buffer (PBS, 2% BSA,
123 0.05% sodium azide). Cells were conjugated with LIVE/DEAD Fixable Near-IR viability dye
124 (Invitrogen, L34975) at 1:1000 dilution in PBS for 5 minutes at room temperature. Finally, cells
125 were washed 3x in cold cell media (RPMI, 10% FBS) before sorting (BD Biosciences, FACSAria
126 Fusion) for live cells. Sorted cells were partitioned into droplets for single-cell RNA-seq via
127 Chromium Next GEM Single-Cell 5' Kit v2 (10x Genomics, 1000263). RNA-seq libraries were
128 prepared according to manufacturer protocols. Libraries were quantified via the Qubit dsDNA HS
129 Assay Kit (Invitrogen, Q32851), quality-checked for fragment sizes via high-sensitivity D5000
130 screentapes (Agilent, 5067-5592), pooled, and sequenced (Illumina, Novaseq-6000,
131 RRID:SCR_016387 and Nextseq-550, RRID:SCR_016381).

132

133 *Single-cell RNA-seq data analysis*

134 Alignment, filtering, counting, and demultiplexing of RNA-seq reads were performed using the
135 Cell Ranger *count* (10x Genomics, version 7.1.0, RRID:SCR_017344). For alignment, the
136 GRCh38 reference genome was appended with the CAR transgene sequence of axicabtagene
137 ciloleucel.

138 Downstream analysis was performed using Seurat[25] (version 4.3.0, RRID:SCR_016341).
139 After converting count matrices and merging all Seurat objects, we filtered cells with >15%
140 mitochondrial reads and 40,000 UMIs to remove debris, doublets, and dead cells. The matrix was
141 normalized using *NormalizeData* with default options. The top 5,000 variable genes found by
142 *FindVariableFeatures* with the default "vst" method were taken as variable genes. Data were
143 centered and scaled using *ScaleData*, with additional regression against (1) the percent of
144 mitochondrial RNA content and (2) difference in cell cycle S-phase and G2M-phase scores.
145 Scaled data were then used for principal component analysis (PCA) using *RunPCA*. Data
146 harmonization to remove patient-specific effects was performed on the principal components
147 using Harmony[26] (version 0.1.1, RRID:SCR_018809) through *RunHarmony*. Top 50 Harmony
148 components were used for Uniform Manifold Approximation and Projection (UMAP)
149 dimensionality reduction via *RunUMAP*. The same harmony components were used to construct
150 the shared nearest neighbor (SNN) graph using *FindNeighbors*, which was then partitioned to
151 identify clusters using *FindClusters* with the "original Louvain" algorithm.

152 Differentially expressed genes were determined using *FindMarkers* in the Seurat package
153 with default parameters. Gene set enrichment analysis and pathway enrichment analysis were
154 carried out using clusterProfiler[27] (version 4.6.2, RRID:SCR_016884) based on pathways from
155 the msigdbr database's built-in msigdbr[28] package (version 7.5.1, RRID:SCR_022870). Gene
156 module scores were calculated for each cell using *AddModuleScore* in Seurat for msigdbr or
157 customized gene sets.

158

159 *Cell lines*

160 The OCI-Ly8 (RRID:CVCL_8803) cell line was obtained from Dr. James L. LaBelle's lab
161 (University of Chicago), the VAL cell line (RRID:CVCL_1819) was obtained from Dr. Justin P.
162 Kline's lab (University of Chicago), the NALM6 cell line was obtained from ATCC (CRL-3273™,
163 RRID:CVCL_0092), and the Lenti-X 293T packaging cell line was obtained from Takara (632180,
164 RRID:CVCL_4401). All cell lines were confirmed to be mycoplasma-negative using the Universal
165 Mycoplasma Detection Kit (ATCC, 30-1012k), with the most recent testing performed in
166 November 2025. All cell lines were used for experiments within three passages after thawing.

167

168 *Lentiviral production and transduction*

169 CD28- or 4-1BB-costimulated anti-CD19 human CARs were designed based on the sequences
170 of axi-cel or liso-cel. The axi-cel sequence was obtained from a previously published sequencing
171 study,[29] while the liso-cel sequence was retrieved from the Global Substance Registration System
172 database (UNII: 7K2YOJ14X0). A GFP-tagged, CD28-costimulated or 4-1BB-costimulated, anti-
173 CD19 human CAR was cloned onto the pHR vector backbone to constitute the transfer plasmid.
174 Plasmids were transfected into the Lenti-X 293T packaging cell line (Takara, 632180,
175 RRID:CVCL_4401) for lentiviral production. In brief, Lenti-X 293T cells were seeded and grown
176 overnight to ~90% confluence. Subsequently, transfer, packaging (psPAX2, Addgene, #12260,
177 RRID:Addgene_12260), and envelope (pMD2.G, Addgene, #12259, RRID:Addgene_12259)
178 plasmids were co-transfected into Lenti-X 293T cells via Lipofectamine 3000 (Invitrogen,
179 L3000001). After 72 hours, the viral supernatant was collected and stored at -80°C until
180 transduction. During transduction, lentiviruses were added to human primary T cells along with
181 protamine sulfate (Millipore Sigma, P3369-10G) to a final concentration of 10 μg/mL. Cells were
182 spinoculated at 800 × *g* for 60 minutes at room temperature. All cell lines were routinely tested
183 for Mycoplasma contamination every 4-6 weeks using a PCR-based assay.

184

185 *CAR T-cell production and culturing*

186 PBMC samples were collected from healthy donors under an Institutional Review Board approved
187 protocol. Cryopreserved human PBMCs were thawed in warm T-cell media (RPMI supplemented
188 with 10% FBS, 1% penicillin/streptomycin, 2 mM L-glutamine, and 50 μM 2-mercaptoethanol).
189 Subsequently, PBMCs were cultured for 3 hours in complete T-cell media (T-cell media
190 supplemented with 50 units/mL of IL-2) in order to allow monocytes to adhere to the culture flask.
191 The non-adhered cells were transferred to a new culture flask. Cells were counted via the LUNA-
192 FL cell counter. T-cell percentage (% $CD3^+$) was calculated by flow cytometry.

193 T cells were seeded in complete T-cell media at 0.75×10^6/mL. CD3/CD28 Dynabeads
194 (Gibco, 11161D) were washed and added at 1:1 ratio. After overnight activation, T cells were
195 transduced with CAR lentiviruses (MOI of 5). The media was refreshed after 24 hours with
196 complete T-cell media dosed with recombinant human IFN-α2 (BioLegend, 592702). T cells were
197 subsequently expanded, and media was refreshed every 2 days.

198

199 *Quantitative reverse transcription PCR*

200 CAR T cells were treated under IFN-I culturing conditions for 24 hours. Then, cells were collected,
201 and stained for viability (Invitrogen, L34975). Live CAR T cells were sorted (BD Biosciences,
202 FACSAria Fusion). Total RNA was extracted using the Monarch Total RNA Miniprep Kit (NEB,
203 T2010S), according to manufacturer protocols. RNA was quantified via the Qubit RNA HS Assay
204 Kit (Invitrogen, Q32852). cDNA was synthesized using the GoScript Reverse Transcription
205 System (Promega, A5000).

206 Quantitative PCR was performed using Taqman Gene Expression Assay (ThermoFisher
207 Scientific, 4331182) and Applied Biosystems TaqMan Universal PCR Master Mix (ThermoFisher
208 Scientific, 4304437), on LightCycler® 96 Instrument (Roche). The cycling conditions were as
209 follows: UNG incubation at 50°C for 2 minutes, initial denaturation at 95°C for 10 minutes, followed

210 by 40 cycles of denaturation at 95°C for 15 seconds and annealing/extension at 60°C for 60
211 seconds. Each sample was run in triplicate.
212 The specific Taqman Gene Expression Assay used were as follows: *ACTB*
213 (Hs01060665_g1), *IRF7* (Hs01014809_g1), *MX1* (Hs00895608_m1), and *ISG15*
214 (Hs01921425_s1). Relative gene expression levels were calculated using the 2^-ΔΔCt method,
215 with *ACTB* serving as the internal control. Statistical analysis was performed using one-way
216 ANOVA followed by a Tukey's post hoc test for significance.
217
218 In vitro *co-culture immunoassays*
219 For all co-culture immunoassays, CAR T cells (E) and luciferized OCI-Ly8 cells (T,
220 RRID:CVCL_8803) were seeded under a fixed E/T ratio. To measure *in vitro* cytotoxicity, co-
221 cultures were established with E/T ratio of 1:1. After 6 hours, One-Glo Luciferase substrate
222 (Promega, E6110) was added to each well. Residual tumor cells were quantified via luciferase
223 activity. As a positive control, target cells were directly lysed with 1% NP-40 (Abcam, ab142227).
224 To measure cytotoxic molecule expression, co-cultures were established with E/T ratio of 1:1 with
225 1× brefeldin A (BioLegend, 420601). After 4 hours, cells were collected for intracellular staining
226 and flow cytometry. To measure cytokine secretion, co-cultures were established with E/T ratio
227 of 1:1. After 24 hours, the culture supernatant was collected and stored. Secreted cytokines were
228 quantified using LEGENDplex immunoassays per manufacturer's protocol (BioLegend). To
229 measure *in vitro* persistence, co-cultures were established with E/T ratio of 1:5. Every three days,
230 cells were counted using Precision Count Beads (BioLegend, 424902) and measured for
231 apoptosis on flow cytometry. Cell media was then refreshed.
232
233 *Flow cytometry*
234 Cells were washed with cold FACS buffer (PBS, 2% BSA, 0.05% sodium azide). Fc receptors
235 were blocked by incubation with Human TruStain FcX (BioLegend, 422301) at 1:50 dilution for 5

236 minutes at 4°C. Then, cells were incubated for 30 minutes at 4°C in the dark with an antibody
237 staining solution for surface antigen staining. Antibodies were used according to manufacturer
238 recommendations. After staining, cells were incubated briefly either with live/dead staining
239 solution or apoptosis staining solution for 10 minutes at room temperature. Then, cells were either
240 washed and resuspended in FACS buffer or resuspended in Annexin V Binding Buffer (BioLegend,
241 422201). Cells were ready for analysis by flow cytometry or intracellular staining.

242 For intracellular staining, cells stained for surface antigens were subject to the BD
243 Fixation/Permeabilization Kit (BD Biosciences, 554714) for cytotoxic molecule staining or True-
244 Nuclear™ Transcription Factor Buffer Set (BioLegend, 424401) for IRF7 staining, following
245 manufacturer recommendations. In brief, cells were fixed in fixation buffer, washed 3× in
246 permeabilization buffer, and incubated for 60 minutes at 4°C in the dark with a staining solution
247 containing antibodies and permeabilization buffer. After staining, cells were washed 2× in
248 permeabilization buffer, 1x in FACS buffer, and resuspended in FACS buffer for analysis by flow
249 cytometry.

250 For Ki-67 staining, cells stained for surface antigens were washed 2× in PBS, fixed in
251 prechilled 70% ethanol overnight, washed 2× in FACS buffer, and incubated for 30 minutes at
252 4°C in the dark with Ki-67 antibody staining solution. After staining, cells were washed 2× in FACS
253 buffer, and resuspended in FACS buffer for analysis by flow cytometry.

254 Flow cytometry was performed on LSRFortessa (BD Biosciences, RRID:SCR_018655) or
255 Aurora (Cytek Biosciences, RRID:SCR_019826). Data were analyzed using FlowJo software
256 (version 10.10.0, RRID:SCR_008520).

257

258 *Antibodies*

259 All antibodies were used according to manufacturer recommendations. APC-anti-IFNAR2 (10359-
260 MM07T-A) was from Sino Biological. All other antibodies originate from BioLegend. For surface
261 staining, AF647-anti-CD3 (clone: UCHT1, 300416, RRID:AB_389332), BV421-anti-CD3 (clone:

262 UCHT1, 300434, RRID:AB_10962690), BV510-anti-CD4 (clone SK3, 344633,
263 RRID:AB_2566016), PerCP/Cy5.5-anti-CD8α (clone SK1, 344709, RRID:AB_2044009), PE-anti-
264 CD45RA (clone HI100, 304107, RRID:AB_314411), BV421-anti-CD45RO (clone UCHL1, 304223,
265 RRID:AB_10898323), AF647-anti-CCR7 (clone G043H7, 353217, RRID:AB_10913812), BV421-
266 anti-PD-1 (clone EH12.2H7, 329919, RRID:AB_10900818), PE/Cy7-anti-LAG-3 (clone 11C3C65,
267 369309, RRID:AB_2629752), PE/Dazzle™ 594-anti-TIGIT (clone A15153G, 372715,
268 RRID:AB_2632930), PE/Cy7-anti-CCR7 (clone G043H7, 353225, RRID:AB_11125576), and
269 BV785-anti-CD62L (clone DREG-56, 304829, RRID:AB_2629516) were used. For intracellular
270 staining, PE/Cy7-anti-granzyme B (clone QA16A02, 372213, RRID:AB_2728380), PE-anti-
271 perforin (clone B-D48, 353303, RRID:AB_10915476), and PE-anti-IRF7 (clone 12G9A36, 656003,
272 RRID:AB_2563006) were used. For live/dead staining, Zombie NIR Fixable Viability Kit (423106)
273 was used in PBS. For apoptosis staining, BV421-Annexin V (640923, RRID:AB_2893503) or
274 PE/Cy7-Annexin V (640950) was diluted in Annexin V Binding Buffer (422201). For Ki-67 staining,
275 PE-anti-Ki-67 (clone Ki-67, 350503, RRID:AB_10660818) was used.
276
277 *Xenograft mouse models*
278 Immunocompromised NOD-*scid* IL2Rgamma^{null} (NSG, Strain #005557) mice were purchased
279 from JAX and maintained at the animal resource center (ARC) of the University of Chicago in
280 accordance with institutional guidelines. Mice were monitored daily. Care and experimental
281 procedures were carried out in line with the Institutional Animal Care and Use Committee (IACUC)
282 approved protocols of the Animal Care Center at the University of Chicago.
283 For the standard xenograft models, 5×10^6 OCI-Ly8-Chili-luc or 5×10^5 NALM6-Chili-luc
284 cells in 100 μL PBS were intravenously injected into 8-12-week-old NSG mice. Mice were
285 randomized prior to CAR T-cell injection. 5×10^5 or 1×10^6 CAR T cells were intravenously injected
286 1 week later for the OCI-Ly8 model or 4 days later for the NALM6 model. For the OCI-Ly8 model
287 to evaluate durable efficacy of CAR T cells, 3×10^6 OCI-Ly8-Chili-luc cells were intravenously

288 injected on day 0, followed by randomization and intravenous injection of 3×10^5 CAR T cells 1
289 week later. Mice were then injected with an additional 3×10^6 OCI-Ly8-Chili-luc cells intravenously
290 10 days after CAR T-cell infusion. Tumor progression was monitored using either IVIS Spectrum
291 (PerkinElmer) or Lago X (Spectral Instruments Imaging) following the intraperitoneal injection of
292 1 mg D-luciferin potassium (PerkinElmer, 122799) in 200 μL PBS. Animals were anesthetized at
293 1.5% isoflurane throughout acquisition. Bioluminescence was quantified with Aura software
294 (Spectral Instruments Imaging). Euthanasia was conducted via CO_2 overdose followed by cervical
295 dislocation upon manifestation of paralysis, impaired mobility, or poor body condition (BCS<2).
296 Group sizes were determined based on prior experience with the xenograft model and expected
297 treatment effect sizes.
298 Blood was collected by cheek bleeding using a 4-mm lancet (Fisher Scientific,
299 NC9922361), and 50 μL was subjected to red blood cell (RBC) lysis using RBC lysis buffer
300 (eBioscience, 00-4300-54). Lysis was quenched with FACS buffer, and cells were washed once
301 with FACS buffer before proceeding to flow staining. Spleens were collected by surgery and gently
302 ground through a 40-μm cell strainer, followed by RBC lysis using RBC lysis buffer (eBioscience,
303 00-4300-54). After stopping the lysis with RPMI supplemented with 10% FBS, cells were washed
304 once more with RPMI + 10% FBS before being subjected to flow staining.
305
306 *Statistical analysis*
307 Statistical tests were performed on R (version 4.2.1, RRID:SCR_001905) or GraphPad Prism 10
308 (version 10.1.1, RRID:SCR_002798). Comparisons between two groups were performed using
309 Wilcoxon rank-sum test or unpaired t-test. Comparisons between more than two groups were
310 performed by either one-way or two-way ANOVA followed by Tukey's correction for multiple
311 comparisons. Survival data were analyzed using the Log-Rank (Mantel-Cox) test.
312

Data availability

All data are available from the authors upon reasonable request.

Code availability

Codes supporting the analyses performed in this study are available at https://github.com/ertingtang/IFN-I-CART.

319 **RESULTS**

320

321 *Enrichment of IFN-I signaling in infusion products of complete responders.*

322 To uncover determinants of therapeutic efficacy, infusion products (IPs) from 8 r/r DLBCL patients
323 treated with CD28-costimulated CD19-directed CAR T-cell therapy (axicabtagene ciloleucel, "axi-
324 cel") at the University of Chicago Medicine were profiled using single-cell sequencing. The cohort
325 included 5 patients who achieved a complete response (CR) at one month post-infusion and
326 another 3 patients who exhibited progressive disease (N-CR) (**Fig. 1A**, Supplementary Table 1).
327 After removing low-quality cells, we obtained 27,879 cells distributed among 7 T-cell clusters (**Fig.**
328 **1B**) based on gene expression (**Fig. 1C**, Supplementary Fig. S1A). No cluster was patient specific
329 (**Fig. 1D**, Supplementary Fig. S1B). The two $CD8^+$ clusters were annotated as central memory
330 (CM, *SELL*$^+$*IL7R*$^+$*TBX21*$^-$*KLRG1*$^-$) or effector memory (EM, *SELL*$^-$*IL7R*$^+$*TBX21*$^+$*KLRG1*$^+$) T cells.
331 The two $CD4^+$ clusters were annotated as memory (Mem, *FOXP3*^{lo}*IL7R*$^+$*CTLA4*^{lo}) or regulatory
332 (Treg, *FOXP3*^{hi}*IL7R*$^-$*CTLA4*^{hi}) T cells. The remaining three clusters consisted of naïve-activated
333 (*SELL*$^+$*IL7R*$^+$*TCF7*$^+$*CD38*$^+$), unconventional (*TRDC*$^+$*NCAM1*$^+$) as a mixture of γδ and natural killer
334 phenotypes, and proliferating (*MKI67*$^+$*TOP2A*$^+$) T cells. No discernable composition differences
335 were found between CR and N-CR patients (**Fig. 1B** and **D**, Supplementary Fig. S1C).

336 Gene set enrichment analysis revealed distinct differences between CR and N-CR T cells.
337 CR T cells were enriched for signatures of type I interferon signaling ("IFNα response"), cytolysis,
338 and leukocyte degranulation, whereas N-CR T cells were enriched for signatures of cell growth,
339 hypoxia, and glycolysis (**Fig. 1E**). Notably, the CR-specific IFNα response signature was enriched
340 in CR T cells across T-cell clusters and individual patients, with the effect-size analysis (Cliff's δ)
341 indicating moderate to strong differences between CR and N-CR groups (**Fig. 1F** and **G**).

342 To validate our discovery of CR-specific IFN-I signaling signature, we tested our findings
343 using an independent and published single-cell transcriptomic dataset from Maus et al. (n = 15
344 patients with lymphoma who received axi-cel, **Fig. 1A**).[12] This cohort included 10 patients who

345 achieved a complete response (CR) and 5 who did not (N-CR), as assessed one-month post-
346 infusion. After filtering out low-quality cells, performing dimensionality reduction, and clustering,
347 we uncovered the same 7 T-cell clusters identified in our own dataset (**Fig. 1H**) based on gene
348 expression (**Fig. 1I**, Supplementary Fig. S2A). No cluster was patient specific (**Fig. 1J**). Notably,
349 expression of ISGs (including *ISG20*, *IFITM1/3*) was upregulated in IPs of CR (Supplementary
350 Fig. S2B). Most importantly, IFNα response signature was enriched in IPs of CR (Supplementary
351 Fig. S2C). The CR-specific enrichment of IFNα response signature was consistently observed
352 across all clusters (except Tregs) and across individual patients, again with effect-size analysis
353 (Cliff's δ) indicating moderate to strong differences between CR and N-CR groups (**Fig. 1K** and
354 **L**).
355 Taken together, findings from the discovery and validation datasets strongly support an
356 association between IFN-I signaling and improved CAR T-cell clinical efficacy.
357
358 *IFN-I signaling increases CAR T-cell cytotoxicity.*
359 Previous studies have demonstrated the immunomodulatory role of T cell-intrinsic IFN-I
360 signaling.[13] For instance, IFN-I signaling promotes cytotoxicity[16], T_h1 polarization[30–32], and central
361 memory phenotype differentiation[17], all of which may be desired CAR T-cell characteristics and
362 potentially explain the differential clinical responses observed in the two patient cohorts. Based
363 on these findings and our bioinformatics analyses, we hypothesized that IFN-I signaling can
364 enhance CAR T-cell efficacy. To test this hypothesis, we generated both CD28- and 4-1BB-
365 costimulated CD19-directed CAR T cells using primary T cells from healthy human donors, based
366 on axicabtagene ciloleucel (axi-cel, **Fig. 2B**) and lisocabtagene maraleucel (liso-cel, **Fig. 2C**)
367 respectively. To induce IFN-I signaling, we treated CAR T cells with exogenous IFN-α2, a highly
368 potent, FDA-approved, and clinically compatible IFN-I subtype, for culturing CAR T cells (**Fig. 2A**).
369 Prior to addition of IFN-α2, we confirmed that CAR T cells globally expressed the type I interferon

370 receptor in a transduction-independent and costimulation-independent manner (Supplementary
371 Fig. S3A and C).

372 Since each downstream target of IFN-I signaling exhibits varying sensitivity to IFN-I
373 concentrations[33], we hypothesized that the IFN-I culturing concentration may affect CAR T-cell
374 functions. To determine the IFN-I concentrations for our study, we initially titrated IFN-α2 on both
375 CD28- and 4-1BB-costimulated CAR T cells and measured intracellular interferon regulatory
376 factor 7 (IRF7), a key ISG[34] (Supplementary Fig. S3B and D). IFN-I signaling reached saturation
377 at concentrations above 3000 IU/mL of IFN-α2, consistent with previous studies.[16,32] We also
378 observed half-maximal IRF7 upregulation at approximately 100-300 IU/mL of IFN-α2.
379 Consequently, we established three culturing conditions: IFN-α2 at saturating concentration
380 ("IFNα-hi", 3000 IU/mL), IFN-α2 near half-maximal effective concentration ("IFNα-lo", 300 IU/mL),
381 and no IFN-α2 ("IFNα-neg", 0 IU/mL). We confirmed that these conditions resulted in
382 concentration-dependent upregulation of ISGs, including *MX1*, *IRF7*, and *ISG15* (Supplementary
383 Fig. S4).

384 CAR T cells were treated based on the three culturing conditions for downstream
385 experimentation (**Fig. 2A**). Briefly, T cells were transduced with the CAR construct one day after
386 activation (day 1). IFN-I treatment was administered from day 2 to day 7, after which IFN-I was
387 completely removed by washing and refreshing the culture medium. Cells were subsequently
388 expanded until day 13 for experiments. Since IFN-I signaling can inhibit viral transduction[35], we
389 chose to add IFN-α2 after CAR transduction, which enabled us to achieve consistent transduction
390 efficiency and expression of both CD28-costimulated (**Fig. 2D** and **F**) and 4-1BB-costimulated
391 CARs (**Fig. 2E** and **H**) across the three culturing conditions. IFN-α2 was also removed on day 7
392 of *ex vivo* expansion to prevent residual cytokine from inducing potential *in vivo* toxicity.[36,37]
393 Between culturing conditions, IFN-I signaling did not affect CD4/CD8 ratios (**Fig. 2G** and **I**),
394 memory phenotypes (Supplementary Fig. S5A-D), or IFN-I receptor expression (Supplementary
395 Fig. S5E-H). Although long-term sustained IFN-I signaling drives T cell exhaustion in tumor

396 microenvironment[18], our short-term IFN-I exposure in *ex vivo* culture does not induce exhaustion
397 (Supplementary Fig. S5I and J). To test cytotoxicity, CAR T cells were co-cultured with OCI-Ly8
398 target cells, a $CD19^+$ human DLBCL cell line. In both CD28- and 4-1BB-costimulated CAR T cells,
399 we observed IFN-I signaling significantly increased CAR T-cell cytotoxicity (**Fig. 2J** and **L**),
400 expression of cytolytic molecules (granzyme B, perforin, **Fig. 2K** and **M**), and secretion of
401 cytokines (IL-2, TNF, IFNγ, **Fig. 2N** and **O**), in a concentration-dependent manner. These findings
402 suggest that IFN-I signaling increases CAR T-cell cytotoxicity.
403
404 *High-strength IFN-I signaling increases apoptosis, whereas low-strength IFN-I signaling does not.*
405 The IFNα-lo condition consistently yielded comparable levels of viable CAR T cells to IFNα-neg
406 controls following manufacturing, whereas the IFNα-hi condition reduced CAR T-cell yield (**Fig.**
407 **3A** and **C**). Given previous reports that IFN-I signaling can inhibit cell proliferation[38], we evaluated
408 whether CAR T-cell proliferation was affected by IFN-I signaling through assessing the
409 proliferation marker, Ki-67. No significant differences in Ki-67 expression were observed across
410 the three culturing conditions, indicating that IFN-I signaling does not impair CAR T-cell
411 proliferation during *ex vivo* expansion (**Fig. 3B** and **D**; Supplementary Fig. S6). Since IFN-I
412 signaling also reportedly promotes T-cell apoptosis[20,21], we next quantified CAR T-cell apoptosis
413 via Annexin V staining. Flow phenotyping revealed that CAR T cells in the IFNα-hi condition
414 trended towards increased apoptosis, whereas those in the IFNα-lo condition did not (**Fig. 3E** and
415 **F**).
416 To further investigate the cellularity and apoptosis of CAR T cells from the three culturing
417 conditions following antigen-specific stimulation, we subsequently quantified cellularity and
418 apoptosis of CAR T cells after stimulation with OCI-Ly8 target cells. Following stimulation, CAR
419 T-cell cellularity from the IFNα-lo and IFNα-neg conditions was statistically indistinguishable (**Fig.**
420 **3G** and **H**). On the other hand, CAR T-cell cellularity from the IFNα-hi condition was significantly
421 depleted compared to the other two conditions. At the timepoint when cellularity declines became

422 apparent (day 6 post-stimulation in the representative data), we observed a corresponding
423 enrichment in apoptosis in CAR T cells from the IFNα-hi condition, but not in those from the IFNα-
424 lo condition (**Fig. 3I** and **J**).

425 Taken together, these findings suggest that high-strength, but not low-strength IFN-I
426 signaling increases CAR T-cell apoptosis, thereby negatively affecting persistence during both *ex*
427 *vivo* expansion and post antigen-specific activation.

428

429 *Low-strength IFN-I signaling increases the efficacy of DLBCL patient-derived CAR T cells*

430 To evaluate the clinical translation potential of our IFN-I enhancement process, we tested IFN-α2
431 with CAR T cells generated from the leukapheresis product of a patient with DLBCL. IFN-I
432 signaling increased CAR T-cell cytotoxicity (**Fig. 3K** and **O**) and cytokine secretion (IL-2, TNF,
433 IFNγ, **Fig. 3L** and **P**) in a dose-dependent manner. Upon stimulation with OCI-Ly8 target cells,
434 CAR T cells from the IFNα-hi condition demonstrated decreased persistence and increased
435 apoptosis, whereas those from the IFNα-lo condition maintained similar persistence compared to
436 IFNα-neg controls without increased apoptosis (**Fig. 3M**, **N**, **Q**, and **R**). Findings were consistent
437 across both CD28- and 4-1BB-costimulated CAR constructs (**Fig. 3K**-**N** compared to **Fig. 3O**-**R**).
438 These data demonstrate that low-strength IFN-I signaling enhances effector function without
439 inducing apoptosis or compromising persistence of patient-derived CAR T cells. The results also
440 pave the way for future clinical translation of our findings.

441

442 *Low-strength IFN-I signaling promotes CAR T-cell treatment efficacy in vivo.*

443 Given that the IFNα-lo condition uniquely increases CAR T-cell functionality (**Fig. 2**) without
444 compromising cell viability (**Fig. 3**) in both CD28- and 4-1BB-costimulated CAR T cells, our data
445 demonstrate that low-strength IFN-I signaling promotes CAR T-cell efficacy *in vitro* by balancing
446 function with persistence. Based on these *in vitro* conclusions, we hypothesized that the IFNα-lo
447 condition uniquely optimizes CAR T-cell treatment efficacy *in vivo*.

448 To test our hypothesis, we analyzed the efficacy of CAR T cells prepared from the three
449 culturing conditions in a xenograft lymphoma mouse model based on the OCI-Ly8 cell line (**Fig.**
450 **4A**). To control for donor-donor heterogeneity, CAR T cells were derived from multiple
451 independent donors (three for CD28-costimulated CAR T cells and two for 4-1BB-costimulated
452 CAR T cells). Across donors, CAR T-cell injection prolonged survival relative to the PBS-only
453 control. For CD28-costimulated CAR T cells with donors 1 and 2, CAR T cells from the IFNα-lo
454 condition significantly prolonged survival and slowed down tumor progression relative to CAR T
455 cells from the IFNα-neg and IFNα-hi conditions (**Fig. 4B** and **C**, Supplementary Fig. S7A). For
456 donor 3, although the differences between CAR T cells from IFNα-lo and IFNα-hi conditions were
457 relatively modest compared to other donors, one mouse treated with CAR T cells from the IFNα-
458 lo condition showed a significantly better and sustained response (Supplementary Fig. S7B and
459 C). For 4-1BB-costimulated CAR T cells with donors 4 and 5, CAR T cells from the IFNα-lo
460 condition consistently yielded superior outcomes compared to CAR T cells from the IFNα-neg and
461 IFNα-hi conditions, leading to improved survival and tumor control (**Fig. 4C** and **D**, Supplementary
462 Fig. S7D). Taken together, our findings support our hypothesis and indicate that CAR T cells
463 generated from the IFNα-lo condition, regardless of costimulatory domain, exhibit enhanced *in*
464 *vivo* efficacy compared to those from IFNα-neg or IFNα-hi conditions across multiple donors.
465
466 *Low-strength IFN-I signaling promotes CAR T-cell efficacy in other CD19$^+$ tumor models.*
467 We hypothesized low-strength IFN-I signaling can also enhance CAR T-cell efficacy against other
468 CD19$^+$ tumors. To test this, we evaluated the cytotoxicity of CAR T cells generated under different
469 IFN-α2 treatment conditions against two additional CD19$^+$ tumor cell lines: VAL (a DLBCL cell
470 line) and NALM6 (a leukemia cell line). Consistently, IFN-I treatment enhanced CAR T-cell
471 cytotoxicity for both CD28- and 4-1BB-costimulated CAR constructs in a dose-dependent manner
472 (**Fig. 5A** and **D**, Supplementary Fig. S8A and D). Moreover, low-strength IFN-I signaling did not

473 increase apoptosis or compromise CAR T-cell persistence, whereas high-strength IFN-I signaling
474 did, as assessed *in vitro* (**Fig. 5B**, **C**, **E**, and **F**, Supplementary Fig. S8B, C, E, and F).
475 Furthermore, in an NALM6-based *in vivo* xenograft leukemia model, both CD28- and 4-
476 1BB-costimulated CAR T cells generated under IFNα-lo conditions outperformed the other
477 conditions, as evidenced by prolonged survival and reduced tumor burden (**Fig. 5G**-**K**). Together,
478 these data suggest that the IFNα-lo approach has broad applicability for enhancing CAR T-cell
479 efficacy against other $CD19^+$ tumors.
480
481 *Low-strength IFN-I signaling promotes durable CAR T-cell efficacy.*
482 To rigorously evaluate the durability of antitumor responses mediated by CAR T cells generated
483 under IFNα-lo conditions, we refined the OCI-Ly8 xenograft model by introducing a secondary
484 tumor challenge following initial tumor control with CAR T-cell therapy. This approach enabled
485 assessment of the sustained therapeutic efficacy of these CAR T cells in the setting of residual
486 or recurrent disease (**Fig. 6A**). CAR T cells generated under IFNα-lo conditions conferred superior
487 survival benefit and tumor control compared with those generated under IFNα-neg conditions
488 (**Fig. 6B**-**D**). This was accompanied by higher levels of CAR T cells in the peripheral blood and
489 spleen at later time points following the second challenge (**Fig. 6E** and **F**), although memory
490 phenotypes were not markedly altered (Supplementary Fig. S9). Collectively, these data suggest
491 that the IFNα-lo approach promotes durable CAR T-cell efficacy.
492 In conclusion, our *in vitro* and *in vivo* studies support a model in which low-strength IFN-I
493 signaling selectively promotes CAR T-cell treatment efficacy (**Fig. 6G**). IFN-I signaling promotes
494 CAR T-cell functionality in a concentration-dependent manner, leading to more effective
495 cytotoxicity, cytokine release, and tumor control. However, at a high enough concentration, IFN-I
496 signaling also increases T-cell apoptosis, leading to reduced yield, poorer persistence, and
497 ineffective tumor control. Although the optimal level of IFN-I signaling may be subject to donor-
498 donor heterogeneity, CAR T cells treated with low-strength IFN-I signaling, regardless of

499 costimulatory domain, consistently exhibit enhanced effector functions against lymphoma and
500 leukemia with durable responses.

501 **DISCUSSION**

502

503 In this study, we leveraged single-cell transcriptomic analyses of patient IPs from two independent
504 datasets, *in vitro* functional and phenotypic analyses, and *in vivo* xenograft mouse studies to
505 establish that low-strength IFN-I signaling during the *ex vivo* CAR T-cell manufacturing process
506 selectively promotes CAR T-cell treatment efficacy *in vivo* in a costimulation-independent manner.
507 Our strategy of harnessing IFN-I signaling to enhance CAR T-cell efficacy is grounded in clinical
508 data and existing literature, while also highlighting IFN-I as an enhancer with significant
509 translational potential for use during the CAR T-cell manufacturing process.

510 There are major attractive qualities that make IFN-I a uniquely promising and translatable
511 enhancer for both CAR T-cell therapy and other emerging cellular therapy modalities. Unlike all
512 other natural and engineered cytokines being developed as CAR T-cell enhancers (including IL-
513 7, IL-10, IL-15, IL-21, Fc-IL-4)[39–43], IFN-Is are uniquely biocompatible drugs with an existing and
514 extensive clinical track record for the treatment of malignancies[22], autoimmune diseases[23], and
515 viral infections[24]. First discovered in the 1950s for their antiviral activities, IFN-I is one of only two
516 cytokines ever approved by the FDA for cancer treatment (the other being IL-2).[44] Biologically,
517 IFN-I elicits a known signaling pathway through the type I interferon receptor to induce antiviral
518 interferon-stimulated genes.[13,15] Their pharmacodynamics and pharmacokinetics have been
519 thoroughly explored in pre-clinical and clinical studies.[45] Importantly, whereas existing cytokines
520 such as IL-15 and IL-21 boost stem cell memory phenotype[39] and persistence[41], respectively, our
521 IFN-I conditioning strategy boosts immediate effector functions, including cytotoxicity and
522 cytokine production. Thus, IFN-I enables a distinct and complementary enhancement strategy
523 that synergizes with the current state of the art. Our novel manufacturing method was
524 mechanistically inspired by bioinformatics findings from clinical biospecimens, allowing it to
525 recapitulate a physiological and clinically relevant phenotype. By utilizing a biologically,
526 pharmacologically, and clinically characterized pharmacophore, our low-strength IFN-I

527 manufacturing approach is both straightforward and safe. Our approach involves adding IFN-I
528 cytokines during the manufacturing process, followed by IFN-I removal before CAR T-cell infusion
529 for treatment. This design fundamentally differs from sustained IFN-I exposure[18], allowing us to
530 avoid T-cell exhaustion and harness the beneficial effects of low-strength IFN-I signaling during
531 *ex vivo* CAR T-cell manufacture. Importantly, restricting IFN-I exposure to the manufacturing
532 process ensures simplicity and compatibility with existing manufacturing methods and CAR
533 constructs, while eliminating potential *in vivo* IFN-I-associated toxicities.

534 In terms of basic biology, we found that IFN-I signaling enhances CAR T-cell cytotoxicity
535 in a dose-dependent manner; however, excessively strong IFN-I signaling also increases
536 apoptosis, thereby reducing persistence. Our findings are compatible with existing literature on T-
537 cell-intrinsic effects of IFN-I signaling. Enhancement of cytotoxicity and type I cytokine secretion
538 among $CD8^+$ and $CD4^+$ T cells after culturing with exogenous IFN-I is well-established.[16,46]
539 Moreover, the field's current understanding is that T-cell-intrinsic IFN-I signaling leads to different
540 consequences, depending on whether TCR stimulation temporally precedes ("in-sequence") or
541 follows ("out-of-sequence") IFN-I signaling.[13,47] In-sequence signaling generally enhances T-cell
542 functions, while out-of-sequence signaling generally does the opposite.[13] In our studies, since T-
543 cell activation (via CD3/CD28 Dynabeads) preceded IFN-I treatment, our CAR T cells were
544 subject to in-sequence signaling under the current paradigm. Moreover, our findings mirror the
545 expected consequences of in-sequence IFN-I signaling. Lastly, the concentration-dependent
546 nature of our model is compatible with other studies demonstrating that different cellular functions
547 exhibit varying sensitivities to IFN-I signaling.[33]

548 Our findings help reconcile previously conflicting reports regarding the role of IFN-I in CAR
549 T-cell function. While some studies report that IFN-I signaling impairs CAR T-cell efficacy[20,21,48],
550 others report beneficial effects[49]. Jung et al.[48] and Evgin et al.[21] report that IFN-I signaling impairs
551 CAR T-cell efficacy. Both studies used IFN-β, which has up to 30-fold higher affinity for the type I
552 interferon receptor compared to IFN-α2.[50] Considering the high-affinity IFN-I subtype and

553 concentrations applied, their experimental conditions align with our IFNα-hi condition, providing a
554 plausible explanation for their detrimental outcomes. Similarly, Harrer et al. report that autocrine
555 IFN-I signaling (through CAR-activation-induced secretion of IFN-α2 or IFN-β) impairs CAR T-cell
556 efficacy.[20] The resulting IFN-I bioactivity in their cell supernatant aligns with our IFNα-hi condition,
557 triggering increased CAR T-cell apoptosis. In contrast, Zhao et al. reported that IFN-I signaling
558 enhances CAR T-cell efficacy.[49] We reason that their beneficial findings reflect a weak
559 endogenous IFN-I stimulus, as no exogenous IFN-I was added in their *in vitro* system. Together,
560 these comparisons highlight how our model, which defines a non-linear relationship between IFN-
561 I signaling strength and CAR T-cell efficacy, provides a unifying framework to reconcile previously
562 conflicting reports.

563 Our study advances the understanding of IFN-I signaling in T cells and lays the foundation
564 for translational applications in CAR T-cell therapies, though several avenues remain for
565 exploration. Since IFN-I signaling enhances CAR T-cell cytokine production (IL-2, TNF, IFN-γ), it
566 may theoretically increase the risk of cytokine release syndrome (CRS) and immune effector cell-
567 associated neurotoxicity syndrome (ICANS).[51] The xenograft mouse model is not suitable for
568 evaluating either toxicities.[52] Any future application of our IFN-I strategy in the clinical trials context
569 should carefully titrate CAR T-cell dosages, consider patient performance status, monitor
570 treatment toxicities, implement evidence-based clinical management (e.g., tocilizumab for CRS,
571 dexamethasone for ICANS), and incorporate rapid reversal mechanisms where appropriate (e.g.,
572 suicide switches for CAR T cells). Furthermore, we tested only two IFN-I concentrations,
573 emphasizing the need for more rigorous dosing studies to determine the optimal therapeutic
574 window. Finally, although our study focused on IFN-α2 due to its clinical relevance, it underscores
575 the broader potential of the IFN-I family, with many subtypes still underexplored and potentially
576 capable of further enhancing CAR T-cell functionality through cytokine modulation.

577 Looking ahead, the simplicity, clinical familiarity, and GMP compatibility of low-strength
578 IFN-I signaling make this strategy readily adoptable in clinical CAR T-cell manufacturing. Although

579 our studies center on CD19-directed CAR T cells and B cell malignancies, our approach is likely
580 generalizable across additional CAR targets and disease settings. These findings provide strong
581 rationale for advancing low-strength IFN-I signaling toward clinical trials evaluation as a scalable
582 and broadly applicable manufacturing strategy to enhance cell therapies.

583 **ACKNOWLEDGEMENTS**

584

585 We thank the NIH New Innovator award (1DP2AI144245), NIH R21AI169159, the American
586 Cancer Society Scholar Award (SG-22-136-01-1BCD), and NIH R61AG090388 for financial
587 support of this research, including support for reagents and personnel (to J.H.). Y.H. was
588 supported by the University of Chicago MSTP Training Grant (T32GM007281). N.W.A. was
589 supported by the University of Chicago MTCR Training Grant (T32CA009594). Flow cytometry
590 was performed at the Cytometry and Antibody Technology Facility at the University of Chicago,
591 which receives financial support from the Cancer Center Support Grant (P30CA014599). Live
592 bioluminescence imaging was performed at the University of Chicago Integrated Small Animal
593 Imaging Research Resource. We thank the UChicago Blood Donation Center for healthy donor
594 PBMCs. We thank Aniruddhsingh Solanki at the Animal Resource Center at University of Chicago
595 for excellent technical assistance. We thank Dr. Alexandra Rojek from Dr. Justin Kline's lab for
596 sharing the VAL cell line. We also acknowledge Ali Rahman for assistance with cell culture,
597 molecular cloning, and the optimization of immunoassay conditions.

AUTHOR CONTRIBUTIONS

E. Tang: Conceptualization, data curation, formal analysis, investigation, validation, methodology, bioinformatics analysis, writing-original draft, writing-review and editing. **Y. Hu**: Conceptualization (original project idea), clinical data collection, data curation, formal analysis, investigation, validation, methodology, writing-original draft, writing-review and editing. **G. Cao**: Conceptualization, investigation, bioinformatics analysis. **D. Nguyen**, **N. W. Asby**, **N. S. Aboelella**, and **H. A. Ruiz**: Investigation and methodology. **X. Cai**, **W. Zhang**, **Y. Zhao**, **L. Xie**, and **X. Chen**: Methodology. **M. R. Bishop**, **P. A. Riedell**, **J. L. LaBelle**, and **J. P. Kline**: Methodology and resources. **J. Huang**: Conceptualization, resources, funding acquisition, supervision, formal analysis, methodology, writing-original draft, writing-review and editing, project administration.

610 **REFERENCES**

611

612 1. Neelapu, S. S. *et al.* Axicabtagene Ciloleucel CAR T-Cell Therapy in Refractory Large B-
613 Cell Lymphoma. *N. Engl. J. Med.* **377**, 2531–2544 (2017).
614 2. Maude, S. L. *et al.* Tisagenlecleucel in Children and Young Adults with B-Cell
615 Lymphoblastic Leukemia. *N. Engl. J. Med.* **378**, 439–448 (2018).
616 3. Rodriguez-Otero, P. *et al.* Ide-cel or Standard Regimens in Relapsed and Refractory
617 Multiple Myeloma. *N. Engl. J. Med.* **388**, 1002–1014 (2023).
618 4. San-Miguel, J. *et al.* Cilta-cel or Standard Care in Lenalidomide-Refractory Multiple
619 Myeloma. *N. Engl. J. Med.* **389**, 335–347 (2023).
620 5. Rossi, J. *et al.* Preinfusion polyfunctional anti-CD19 chimeric antigen receptor T cells are
621 associated with clinical outcomes in NHL. *Blood* **132**, 804–814 (2018).
622 6. Fraietta, J. A. *et al.* Determinants of response and resistance to CD19 chimeric antigen
623 receptor (CAR) T cell therapy of chronic lymphocytic leukemia. *Nat. Med.* **24**, 563–571
624 (2018).
625 7. Deng, Q. *et al.* Characteristics of anti-CD19 CAR T cell infusion products associated with
626 efficacy and toxicity in patients with large B cell lymphomas. *Nat. Med.* **26**, 1878–1887
627 (2020).
628 8. Finney, O. C. *et al.* CD19 CAR T cell product and disease attributes predict leukemia
629 remission durability. *J. Clin. Invest.* **129**, 2123–2132 (2019).
630 9. Good, Z. *et al.* Post-infusion CAR TReg cells identify patients resistant to CD19-CAR
631 therapy. *Nat. Med.* **28**, 1860–1871 (2022).
632 10. Schuster, S. J. *et al.* Tisagenlecleucel in adult relapsed or refractory diffuse large B-cell
633 lymphoma. *N. Engl. J. Med.* **380**, 45–56 (2019).
634 11. Cheng, J. *et al.* Understanding the Mechanisms of Resistance to CAR T-Cell Therapy in
635 Malignancies. *Frontiers in Oncology* vol. 9 1237 (2019).

636 12. Haradhvala, N. J. *et al.* Distinct cellular dynamics associated with response to CAR-T
637 therapy for refractory B cell lymphoma. *Nat. Med.* **28**, 1848–1859 (2022).
638 13. Crouse, J., Kalinke, U. & Oxenius, A. Regulation of antiviral T cell responses by type I
639 interferons. *Nature Reviews Immunology* vol. 15 231–242 (2015).
640 14. Musella, M., Manic, G., De Maria, R., Vitale, I. & Sistigu, A. Type-I-interferons in infection
641 and cancer: Unanticipated dynamics with therapeutic implications. *Oncoimmunology* **6**,
642 1–12 (2017).
643 15. Ning, S., Pagano, J. S. & Barber, G. N. IRF7: Activation, regulation, modification and
644 function. *Genes and Immunity* vol. 12 399–414 (2011).
645 16. Curtsinger, J. M., Valenzuela, J. O., Agarwal, P., Lins, D. & Mescher, M. F. Cutting Edge:
646 Type I IFNs Provide a Third Signal to CD8 T Cells to Stimulate Clonal Expansion and
647 Differentiation. *J. Immunol.* **174**, 4465–4469 (2005).
648 17. Ramos, H. J. *et al.* Reciprocal responsiveness to interleukin-12 and interferon-α specifies
649 human CD8+ effector versus central memory T-cell fates. *Blood* **113**, 5516–5525 (2009).
650 18. Lukhele, S. *et al.* The transcription factor IRF2 drives interferon-mediated CD8+ T cell
651 exhaustion to restrict anti-tumor immunity. *Immunity* **55**, 2369-2385.e10 (2022).
652 19. Sumida, T. S. *et al.* Type I interferon transcriptional network regulates expression of
653 coinhibitory receptors in human T cells. *Nat. Immunol.* **23**, 632–642 (2022).
654 20. Harrer, D. C. *et al.* CAR Triggered Release of Type-1 Interferon Limits CAR T-Cell
655 Activities by an Artificial Negative Autocrine Loop. *Cells* **11**, (2022).
656 21. Evgin, L. *et al.* Oncolytic virus-derived type I interferon restricts CAR T cell therapy. *Nat.*
657 *Commun.* **11**, 1–15 (2020).
658 22. Musella, M., Manic, G., De Maria, R., Vitale, I. & Sistigu, A. Type-I-interferons in infection
659 and cancer: Unanticipated dynamics with therapeutic implications. *Oncoimmunology* **6**,
660 1–12 (2017).
661 23. Jakimovski, D., Kolb, C., Ramanathan, M., Zivadinov, R. & Weinstock-Guttman, B.

662 Interferon β for Multiple Sclerosis. *Cold Spring Harb. Perspect. Med.* **8**, 1–19 (2018).
663 24. Li, S. F. *et al.* Type i interferons: Distinct biological activities and current applications for
664 viral infection. *Cellular Physiology and Biochemistry* vol. 51 2377–2396 (2018).
665 25. Hao, Y. *et al.* Integrated analysis of multimodal single-cell data. *Cell* **184**, 3573-3587.e29
666 (2021).
667 26. Korsunsky, I. *et al.* Fast, sensitive and accurate integration of single-cell data with
668 Harmony. *Nat. Methods* **16**, 1289–1296 (2019).
669 27. Wu, T. *et al.* clusterProfiler 4.0: A universal enrichment tool for interpreting omics data.
670 *Innovation* **2**, (2021).
671 28. Subramanian, A. *et al.* Gene set enrichment analysis: A knowledge-based approach for
672 interpreting genome-wide expression profiles. *Proc. Natl. Acad. Sci. U. S. A.* **102**, 15545–
673 15550 (2005).
674 29. Cao, G. *et al.* Two-stage CD8+ CAR T-cell differentiation in patients with large B-cell
675 lymphoma. *Nat. Commun.* **16**, 4205 (2025).
676 30. Cho, S. S. *et al.* Activation of STAT4 by IL-12 and IFN-alpha: evidence for the
677 involvement of ligand-induced tyrosine and serine phosphorylation. *J. Immunol.* **157**,
678 (1996).
679 31. Huber, J. P., Ramos, H. J., Gill, M. A. & Farrar, J. D. Cutting Edge: Type I IFN Reverses
680 Human Th2 Commitment and Stability by Suppressing GATA3. *J. Immunol.* **185**, 813–
681 817 (2010).
682 32. Ramgolam, V. S., Sha, Y., Jin, J., Zhang, X. & Markovic-Plese, S. IFN-β Inhibits Human
683 Th17 Cell Differentiation. *J. Immunol.* **183**, 5418–5427 (2009).
684 33. Mendoza, J. L. *et al.* The IFN-λ-IFN-λR1-IL-10Rβ Complex Reveals Structural Features
685 Underlying Type III IFN Functional Plasticity. *Immunity* **46**, 379–392 (2017).
686 34. Marie, I., Durbin, J. & Levy, D. Differential viral induction of distinct interferon-alpha genes
687 by positive feedback through interferon regulatory factor-7. *EMBO J.* **17**, 6660–6669

688 (1998).
689 35. Durgin, J., Sannecy, A., Kelly, A., O'Connor, R. S. & Ghassemi, S. Type I Interferon
690 Blockade Enhances Transduction Efficiency and Efficacy of Non-Activated CAR T Cells.
691 *Blood* **142**, 6830–6830 (2023).
692 36. Trinchieri, G. Type I interferon: Friend or foe? *J. Exp. Med.* **207**, 2053–2063 (2010).
693 37. Quesada, J. R., Talpaz, M., Rios, A., Kurzrock, R. & Gutterman, J. U. Clinical toxicity of
694 interferons in cancer patients: A review. *J. Clin. Oncol.* **4**, 234–243 (1986).
695 38. Cheon, H. J., Wang, Y., Wightman, S. M., Jackson, M. W. & Stark, G. R. How cancer
696 cells make and respond to interferon-I. *Trends in Cancer* **9**, 83–92 (2023).
697 39. Alizadeh, D. *et al.* IL15 enhances CAR-T cell antitumor activity by reducing mTORC1
698 activity and preserving their stem cell memory phenotype. *Cancer Immunol. Res.* **7**, 759–
699 772 (2019).
700 40. Li, L. *et al.* Transgenic expression of IL-7 regulates CAR-T cell metabolism and enhances
701 in vivo persistence against tumor cells. *Sci. Rep.* **12**, 1–14 (2022).
702 41. Štach, M. *et al.* Inducible secretion of IL-21 augments anti-tumor activity of piggyBac-
703 manufactured chimeric antigen receptor T cells. *Cytotherapy* **22**, 744–754 (2020).
704 42. Zhao, Y. *et al.* IL-10-expressing CAR T cells resist dysfunction and mediate durable
705 clearance of solid tumors and metastases. *Nat. Biotechnol.* (2024) doi:10.1038/s41587-
706 023-02060-8.
707 43. Feng, B. *et al.* The type 2 cytokine Fc–IL-4 revitalizes exhausted CD8+ T cells against
708 cancer. *Nature* **634**, (2024).
709 44. Berraondo, P. *et al.* Cytokines in clinical cancer immunotherapy. *Br. J. Cancer* **120**, 6–15
710 (2019).
711 45. Buchwalder, P., Buclin, T., Trinchard, I., Munafo, A. & Biollaz, J. Pharmacokinetics and
712 Pharmacodynamics of IFN-b1a in Healthy Volunteers. *J. Interf. Cytokine Res.* **20**, 857–
713 866 (2000).

714 46. Davis, A. M., Ramos, H. J., Davis, L. S. & Farrar, J. D. Cutting Edge: A T-bet-
715 Independent Role for IFN-α/β in Regulating IL-2 Secretion in Human CD4 + Central
716 Memory T Cells. *J. Immunol.* **181**, 8204–8208 (2008).
717 47. van Boxel-Dezaire, A. H. H., Rani, M. R. S. & Stark, G. R. Complex Modulation of Cell
718 Type-Specific Signaling in Response to Type I Interferons. *Immunity* **25**, 361–372 (2006).
719 48. Jung, I. Y. *et al.* Type I Interferon Signaling via the EGR2 Transcriptional Regulator
720 Potentiates CAR T Cell–Intrinsic Dysfunction. *Cancer Discov.* **13**, 1636–1655 (2023).
721 49. Zhao, Z. *et al.* Structural Design of Engineered Costimulation Determines Tumor
722 Rejection Kinetics and Persistence of CAR T Cells. *Cancer Cell* **28**, 415–428 (2015).
723 50. Ng, C. T., Mendoza, J. L., Garcia, K. C. & Oldstone, M. B. A. Alpha and Beta Type 1
724 Interferon Signaling: Passage for Diverse Biologic Outcomes. *Cell* **164**, 349–352 (2016).
725 51. Xiao, X. *et al.* Mechanisms of cytokine release syndrome and neurotoxicity of CAR T-cell
726 therapy and associated prevention and management strategies. *J. Exp. Clin. Cancer*
727 *Res.* **40**, (2021).
728 52. Duncan, B. B., Dunbar, C. E. & Ishii, K. Applying a clinical lens to animal models of CAR-
729 T cell therapies. *Mol. Ther. Methods Clin. Dev.* **27**, 17–31 (2022).
730

MAIN FIGURES AND LEGENDS

Figure 1. Enrichment of IFN-I signaling in infusion products of complete responders.
A, Cartoon depicting study design of single-cell analysis on infusion products of patients who received axi-cel from discovery and validation datasets. CR, complete responder, N-CR, non-complete responder. **B,** UMAP demonstrating 7 T-cell clusters (proliferating, Naïve-activated, $CD4^+$ Memory, Treg, $CD8^+$ central memory, $CD8^+$ effector memory, unconventional) in infusion products from discovery dataset. No patient-specific or response-specific clusters were found. **C,** Violin plots depicting normalized expression levels of representative markers for each cluster. **D,** Stacked bar graphs depicting T-cell cluster proportions for each patient in discovery dataset. **E,** Gene set enrichment analysis comparing CR and N-CR T cells. For each gene set, direction and statistical significance of enrichment are indicated by the circle's color and size, respectively. **F,** Tilemap depicting scaled IFNα response signature scores in each T-cell cluster across patients. **G,** Box plots depicting IFNα-response signature scores for CR and N-CR T cells within each T-cell cluster. Each dot represents one patient. Effect sizes were calculated using Cliff's δ, and statistical significance was assessed using the Wilcoxon rank-sum test. **H,** UMAP demonstrating 7 T-cell clusters in infusion products from validation dataset from Maus et al. **I,** Violin plots depicting normalized expression levels of representative markers for each cluster. **J,** Stacked bar graphs depicting T-cell cluster proportions for each patient in validation dataset. **K,** Tilemap depicting scaled signature scores of IFNα response gene sets in each T-cell cluster across patients. No Treg was found in P17 infusion products, colored in gray. **L,** Box plots depicting IFNα-response signature scores for CR and N-CR T cells within each T-cell cluster. Each dot represents one patient. Effect sizes were calculated using Cliff's δ, and statistical significance was assessed using the Wilcoxon rank-sum test.

Figure 2. IFN-I signaling increases CAR T-cell cytotoxicity.
A, Workflow of CAR T-cell *ex vivo* generation, treatment, and culturing. Both CD28- (axi-cel-based) and 4-1BB-costimulated (liso-cel-based) CAR T cells were generated for analysis. **B** and **C,** CD28- or 4-1BB-costimulated CAR designs based on the construct used in axicabtagene ciloleucel (**B**) or lisocabtagene maraleucel, respectively (**C**). **D** and **E,** Representative flow plots depicting gating for CAR expression (top) and T-cell lineages (bottom) in CD28-costimulated (**D**) and 4-1BB-costimulated (**E**) CAR T cells. CAR T cells were gated as live $CD3^+meGFP^+$ cells. **F** and **H,** Transduction percentage as measured by meGFP fluorescence among T cells from each culturing condition in CD28-costimulated (**F**, n=3) and 4-1BB-costimulated (**H**, n=3) CAR T cells. **G** and **I,** Stacked bar plots comparing CD8 vs CD4 proportions in CD28-costimulated (**G**, n=3) and 4-1BB-costimulated (**I**, n=3) CAR T cells. **J**-**M,** Cytotoxicity of CD28-costimulated (**J**-**K**) and 4-1BB-costimulated (**L**-**M**) CAR T cells. **J** and **L,** Direct cytotoxicity against firefly luciferase-expressing OCI-Ly8 target cells at E/T ratio of 1:1 via 6-hr bioluminescence assay (n=5). **K** and **M,** Intracellular staining for granzyme B (right) and perforin (left) after 4-hr of coculture with OCI-Ly8 at E/T ratio of 1:1 as measured by flow cytometry (n=3). **N** and **O,** Concentration of cytokines secreted by CD28-costimulated (**N**) and 4-1BB-costimulated (**O**) CAR T cells into the supernatant after 24-hr of coculture with OCI-Ly8 at E/T ratio of 1:1 as measured by ELISA (n=5). From left to right, IL-2, TNF, and IFNγ. All data are shown as mean ± SEM of n experimental replicates from a representative donor. Results are representative of independent experiments using CAR T cells from 3 different donors. Statistical analysis were performed via one-way (**F**, **H**, **J**-**O**) or two-way (**G** and **I**) ANOVA with Tukey's correction for multiple comparisons.

Figure 3. High-strength IFN-I signaling increases apoptosis, whereas low-strength IFN-I signaling does not.
A and **C,** Relative counts of live CAR T cells from the three culturing conditions after CAR T-cell manufacturing in CD28-costimulated (**A**, n=5) and 4-1BB-costimulated (**C**, n=6) CAR T cells.

782 Counts were normalized to the IFNα-neg condition. **B** and **D,** Proliferation of CAR T cells from the
783 three culturing conditions in CD28-costimulated (**B**, n=3) and 4-1BB-costimulated (**D**, n=3) CAR
784 T cells. Left, representative flow plots depicting gating for Ki-67$^+$ proliferating CAR T cells at the
785 day when IFNα was removed. Right, Ki-67$^+$ proliferating cell proportions among CAR T cells. Non-
786 activated T cells from human PBMCs were used as a biological control for gating. **E** and **F,**
787 Apoptosis of CAR T cells from the three culturing conditions after CAR T-cell manufacturing in
788 CD28-costimulated (**E**, n=5) and 4-1BB-costimulated (**F**, n=6) CAR T cells. Left, representative
789 flow plots depicting gating for viable (L/D$^-$Annexin V$^-$), early apoptotic (L/D$^-$Annexin V$^+$), and dead
790 (L/D$^+$Annexin V$^+$) cells among CAR T cells. Right, staining for Annexin V positivity among live
791 CAR T cells. **G** and **H,** Line graphs depicting viable CAR T-cell cellularity of CD28-costimulated
792 (**G**, n=3) and 4-1BB-costimulated (**H**, n=3) CAR T cells *in vitro* following coculture with OCI-Ly8
793 at E/T ratio of 1:5. **I** and **J,** Apoptosis of CD28-costimulated CAR T cells (**I**, n=3) and 4-1BB-
794 costimulated CAR T cells (**J**, n=3) from the three culturing conditions at day 6 after coculture with
795 OCI-Ly8 cells at E/T ratio of 1:5. Left, representative flow plots depicting gating for viable (L/D$^-$
796 Annexin V$^-$), early apoptotic (L/D$^-$Annexin V$^+$), and dead (L/D$^+$Annexin V$^+$) cells among the three
797 culturing conditions. Right, staining for Annexin V positivity among live CAR T cells. **K-R,** *In vitro*
798 data of CAR T cells derived from DLBCL patient leukapheresis products. **K** and **O,** Cytotoxicity of
799 CD28-costimulated (**K**, n=4) and 4-1BB-costimulated (**O**, n=4) CAR T cells. **L** and **P,**
800 Concentration of cytokines secreted by CD28-costimulated (**L**, n=5) and 4-1BB-costimulated (**P**,
801 n=5) CAR T cells into the supernatant after 24-hr of coculture with OCI-Ly8 at E/T ratio of 1:1 as
802 measured by ELISA. From left to right, IL-2, TNF, and IFNγ. **M** and **Q,** Line graphs depicting viable
803 CAR T-cell cellularity of CD28-costimulated (**M**, n=3) and 4-1BB-costimulated (**Q**, n=3) CAR T
804 cells *in vitro* following coculture with OCI-Ly8 at E/T ratio of 1:5. **N** and **R,** Apoptosis of CD28-
805 costimulated CAR T cells (**N**, n=3) and 4-1BB-costimulated CAR T cells (**R**, n=3) from the three
806 culturing conditions at the time points when cellularity declined in (**M**) and (**Q**): day 9 for (**N**) and
807 day 6 for (**R**) at an E:T ratio of 1:5. All data are shown as mean ± SEM of n experimental replicates
808 from a representative donor. **A-J** show results representative of independent experiments using
809 CAR T cells from 3 donors. Statistical analysis were performed via one-way (**A-F**, **I-J**, **K-L**, **N-P**,
810 and **R**) or two-way (**G**, **H**, **M**, **Q**) ANOVA with Tukey's correction for multiple comparisons.
811
812 **Figure 4. Low-strength IFN-I signaling promotes CAR T-cell treatment efficacy *in vivo*.**
813 **A,** Schematic depicting timeline for NSG mouse model based on OCI-Ly8 lymphoma cell line.
814 Seven days following OCI-Ly8 injection, mice were randomly divided into groups that were treated
815 with either PBS or CAR T cells from the three culturing conditions. **B** and **C,** Kaplan-Meier analysis
816 of survival of OCI-Ly8-bearing mice treated with PBS or 5×10^5 CD28-costimulated CAR T cells
817 from various culture conditions. CAR T cells were generated from donor 1 (**B**, n=8,12,13,8), and
818 donor 2 (**C**, n=5,5,4,4). **D** and **E,** Kaplan-Meier analysis of survival of OCI-Ly8-bearing mice
819 treated with PBS or 5×10^5 (**D**) or 1×10^6 (**E**) 4-1BB-costimulated CAR T cells from various culture
820 conditions. CAR T cells were generated from donor 4 (**D**, n=6,6,6,6), and donor 5 (**E**, n=4,5,5,5).
821 Statistical analysis were performed by log-rank (Mantel-Cox) test.
822
823 **Figure 5. Low-strength IFN-I signaling promotes CAR T-cell efficacy in a leukemia model.**
824 **A** and **D,** Direct cytotoxicity of CD28-costimulated (**A**, n=3) and 4-1BB-costimulated (**D**, n=3) CAR
825 T cells against firefly luciferase-expressing NALM6 target cells at E/T ratio of 1:1 via 6-hr
826 bioluminescence assay. **B** and **E,** Line graphs depicting viable CD28-costimulated (**B**, n=3) and
827 4-1BB-costimulated (**E**, n=3) CAR T-cell cellularity *in vitro* following coculture with NALM6 at E/T
828 ratio of 1:5. **C** and **F,** Apoptosis of CD28-costimulated (**C**, n=3) and 4-1BB-costimulated (**F**, n=3)
829 CAR T cells from the three culturing conditions at the time points when cellularity declined in (**B**)
830 and (**E**). Day 6 and day 3 after coculture, respectively. **G,** Schematic depicting timeline for NSG
831 mouse model based on NALM6 leukemia cell line. **H** and **I,** Kaplan-Meier analysis of survival of
832 NALM6-bearing mice treated with PBS, 5×10^5 CD28-costimulated CAR T cells, or 1×10^6 4-1BB-

833 costimulated CAR T cells, generated from a healthy donor under the three IFNα culturing
834 conditions. **H**, mice treated with PBS or 5×10^5 CD28-costimulated CAR T cells (n=8,8,8,8). **I,** mice
835 treated with PBS or 1×10^6 4-1BB-costimulated CAR T cells (n=8,9,9,9). The PBS-treated mice in
836 **H** and **I** were the same cohort and were used as a shared control in the same experiment. **J** and
837 **K,** Representative bioluminescence imaging of tumor burden in mice shown in **H** (**J**) and **I** (**K**)
838 (top), with corresponding quantification of bioluminescence (bottom). Statistical analysis were
839 performed via one-way (**A**, **C**, **D**, and **F**) or two-way (**B** and **E**) ANOVA with Tukey's correction for
840 multiple comparisons, or log-rank (Mantel-Cox) test (**H** and **I**). **A**-**F**, All data are shown as mean ±
841 SEM of n experimental replicates from a representative donor. Results are representative of
842 independent experiments using CAR T cells from 3 different donors.
843
844 **Figure 6. Low-strength IFN-I signaling promotes durable CAR T-cell efficacy.**
845 **A,** Schematic depicting timeline for OCI-Ly8-based xenograft tumor model used to assess durable
846 CAR T-cell efficacy. **B,** Kaplan-Meier analysis of survival of OCI-Ly8-bearing mice treated with
847 PBS or 3×10^6 CD28-costimulated CAR T cells generated from a healthy donor under 2 IFNα
848 culturing conditions (n=4,7,7). **C** and **D,** Representative bioluminescence imaging of tumor burden
849 in mice shown in **B**, along with additional CAR T-cell-treated mice used for spleen collection (**C**,
850 n=4,12,12), and corresponding quantification of bioluminescence signals for mice in (**B**, bottom,
851 n=4,7,7). **E,** Longitudinal quantification of CAR^+ cells in 50 μL peripheral blood from mice in **C**. **F,**
852 Quantification of CAR^+ cells in the spleen collected at day 27 from mice in **C**. **G,** Cartoon
853 summarizing effects of IFN-I signaling on CAR T cells at different doses. Statistical analysis were
854 performed by log-rank (Mantel-Cox) test (**B**), two-way (**E**) ANOVA with Tukey's correction for
855 multiple comparisons, or unpaired t-test (**F**).

Figure 1. Enrichment of IFN-I signaling in infusion products of complete responders.

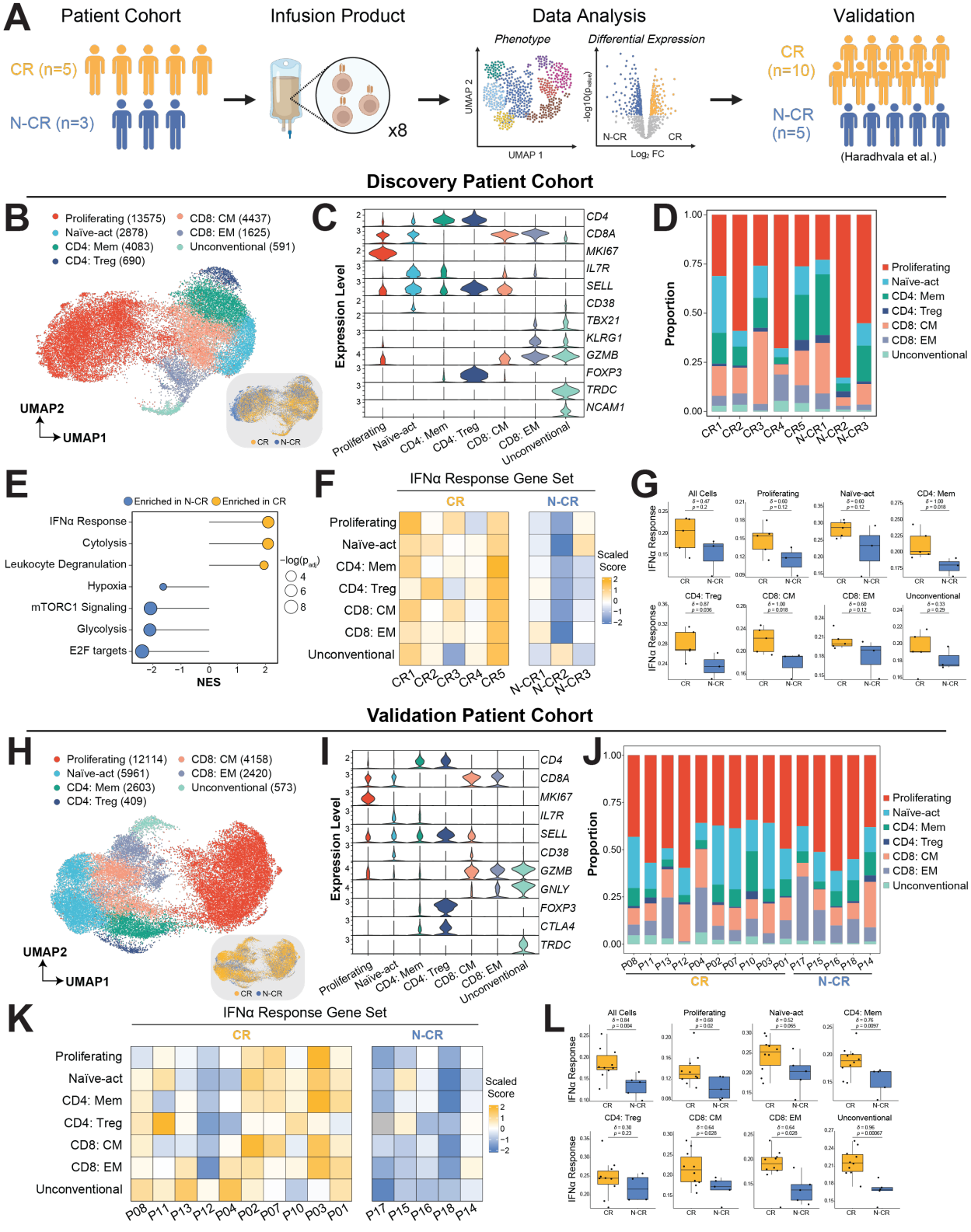

858 **Figure 2. IFN-I signaling increases CAR T-cell cytotoxicity.**

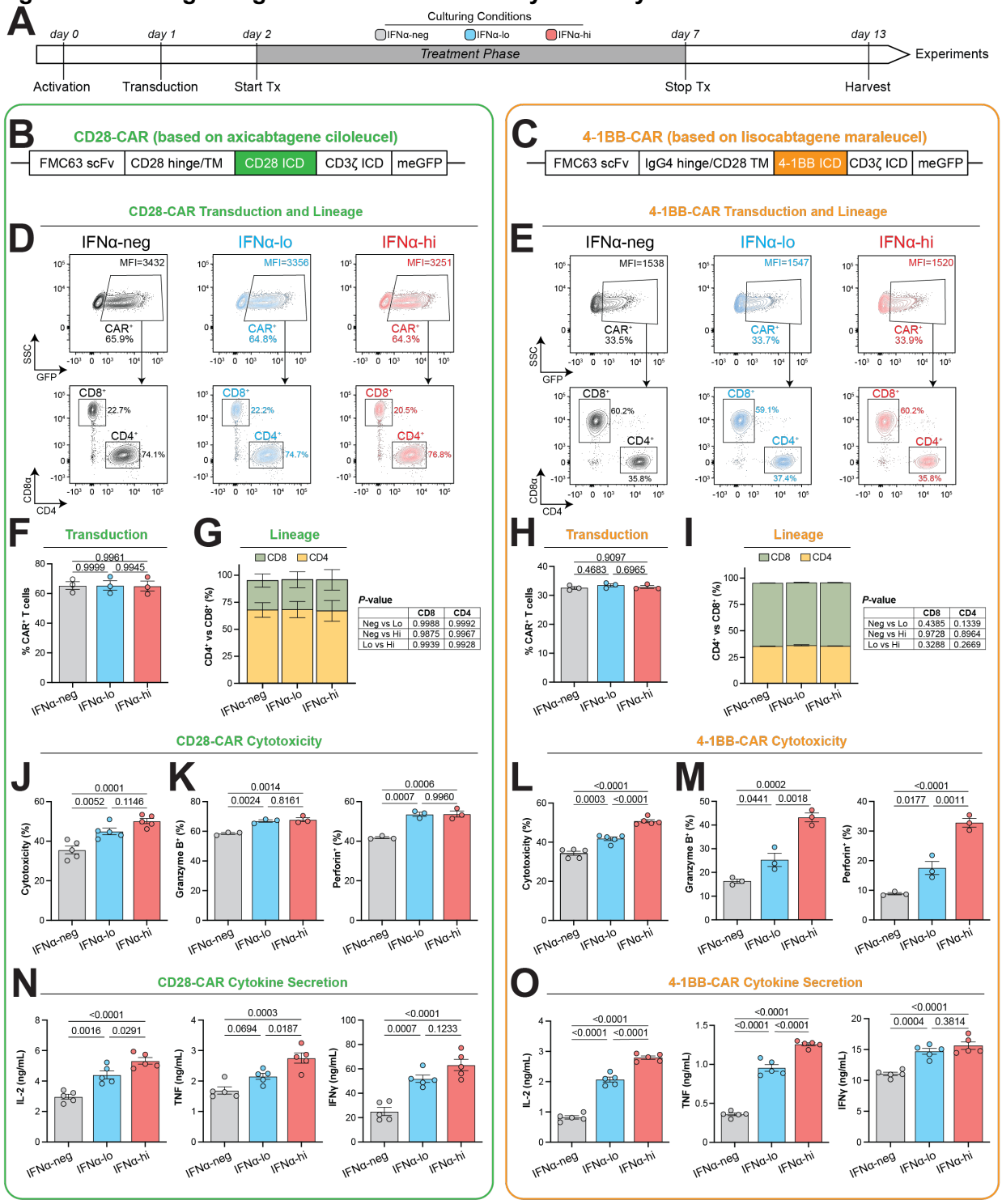

859

Figure 3. High-strength IFN-I signaling increases apoptosis, whereas low-strength IFN-I signaling does not.

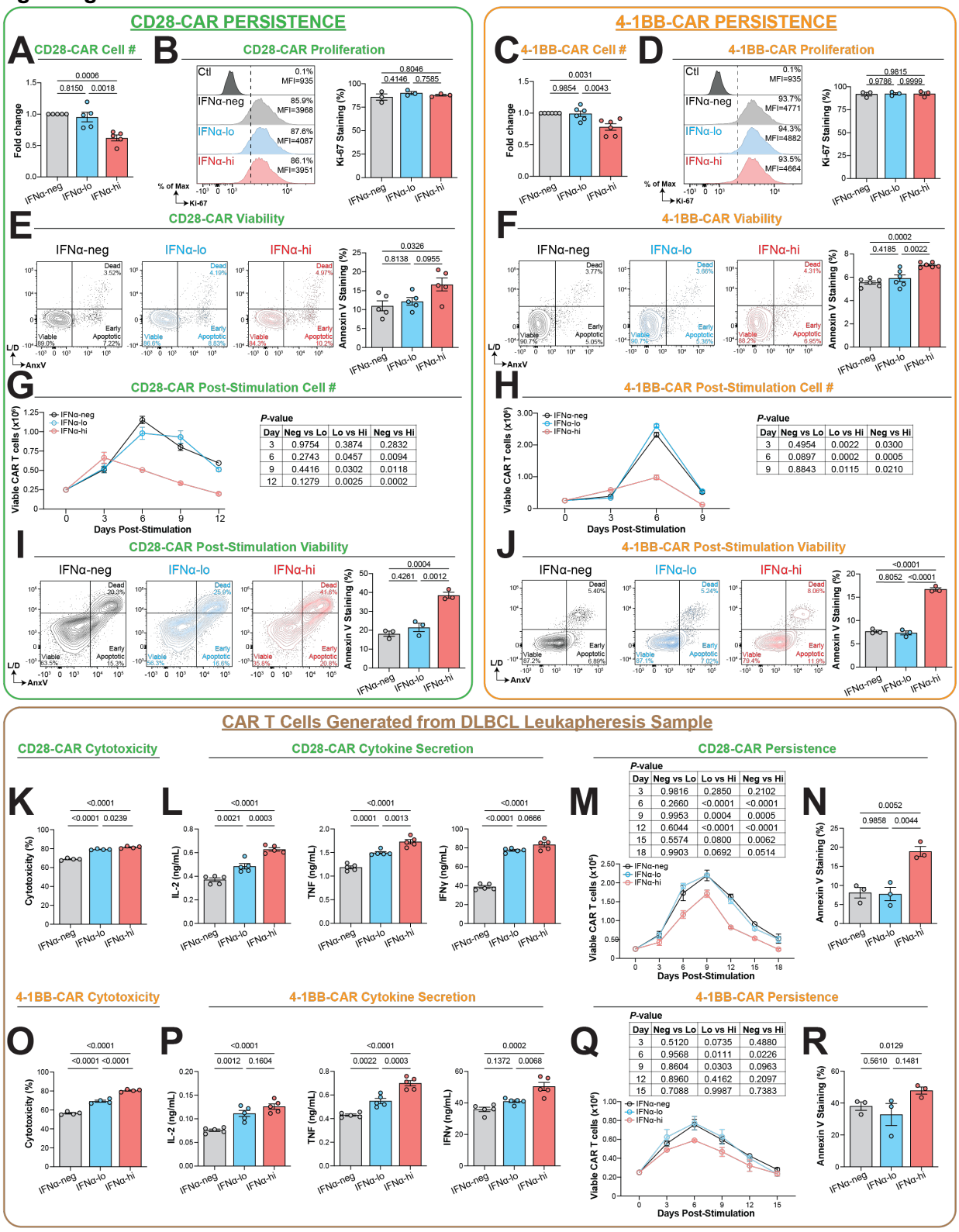

863 **Figure 4. Low-strength IFN-I signaling promotes CAR T-cell treatment efficacy *in vivo*.**

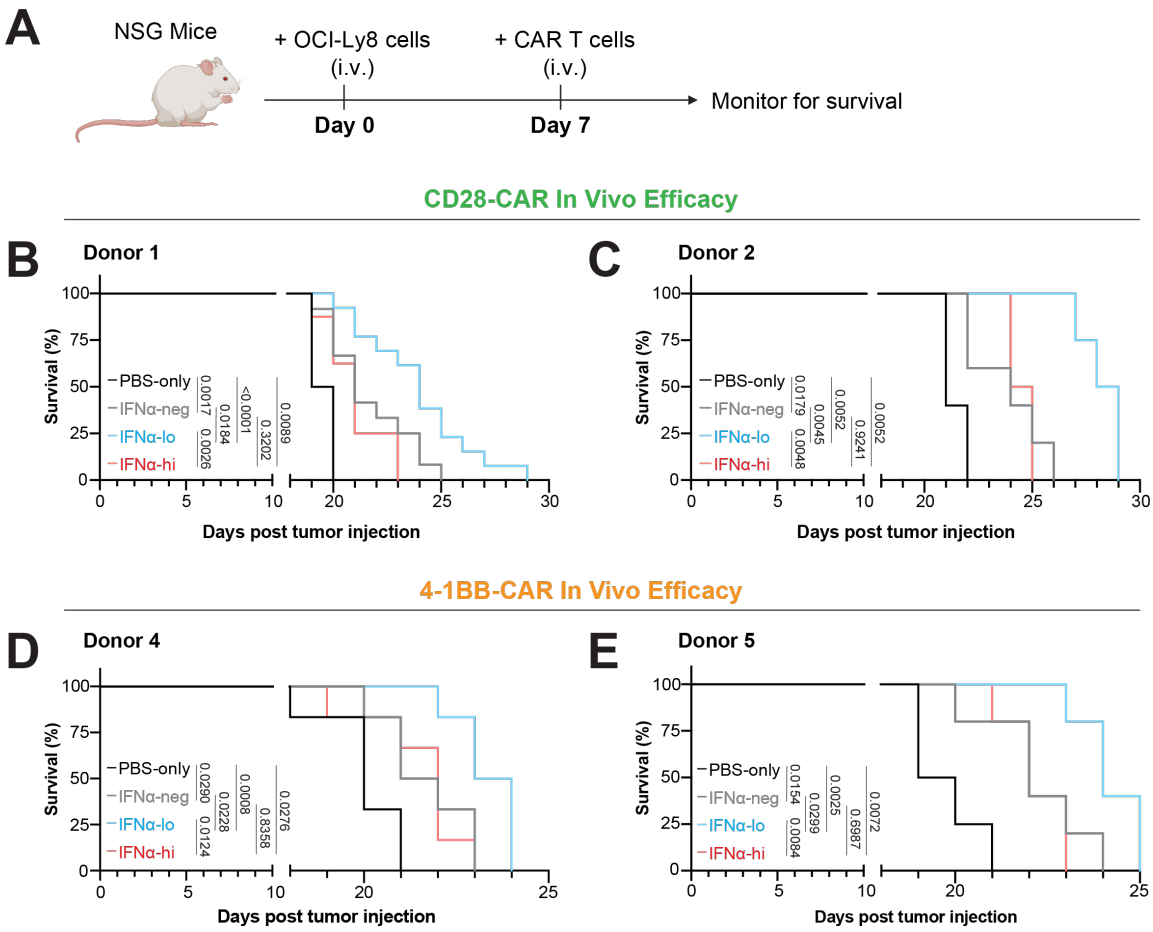

864

Figure 5. Low-strength IFN-I signaling promotes CAR T-cell efficacy in a leukemia model.

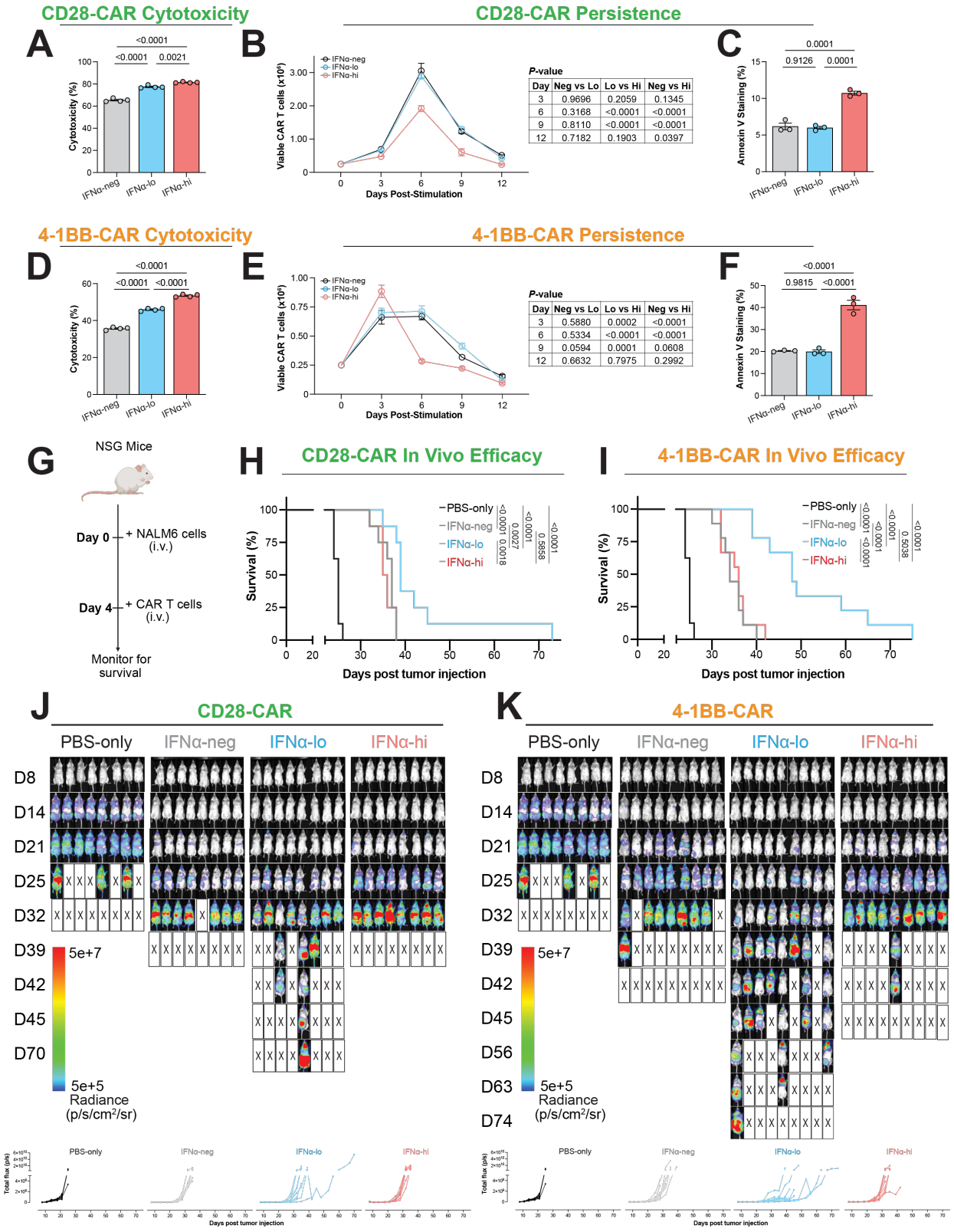

867 **Figure 6. Low-strength IFN-I signaling promotes durable CAR T-cell efficacy.**

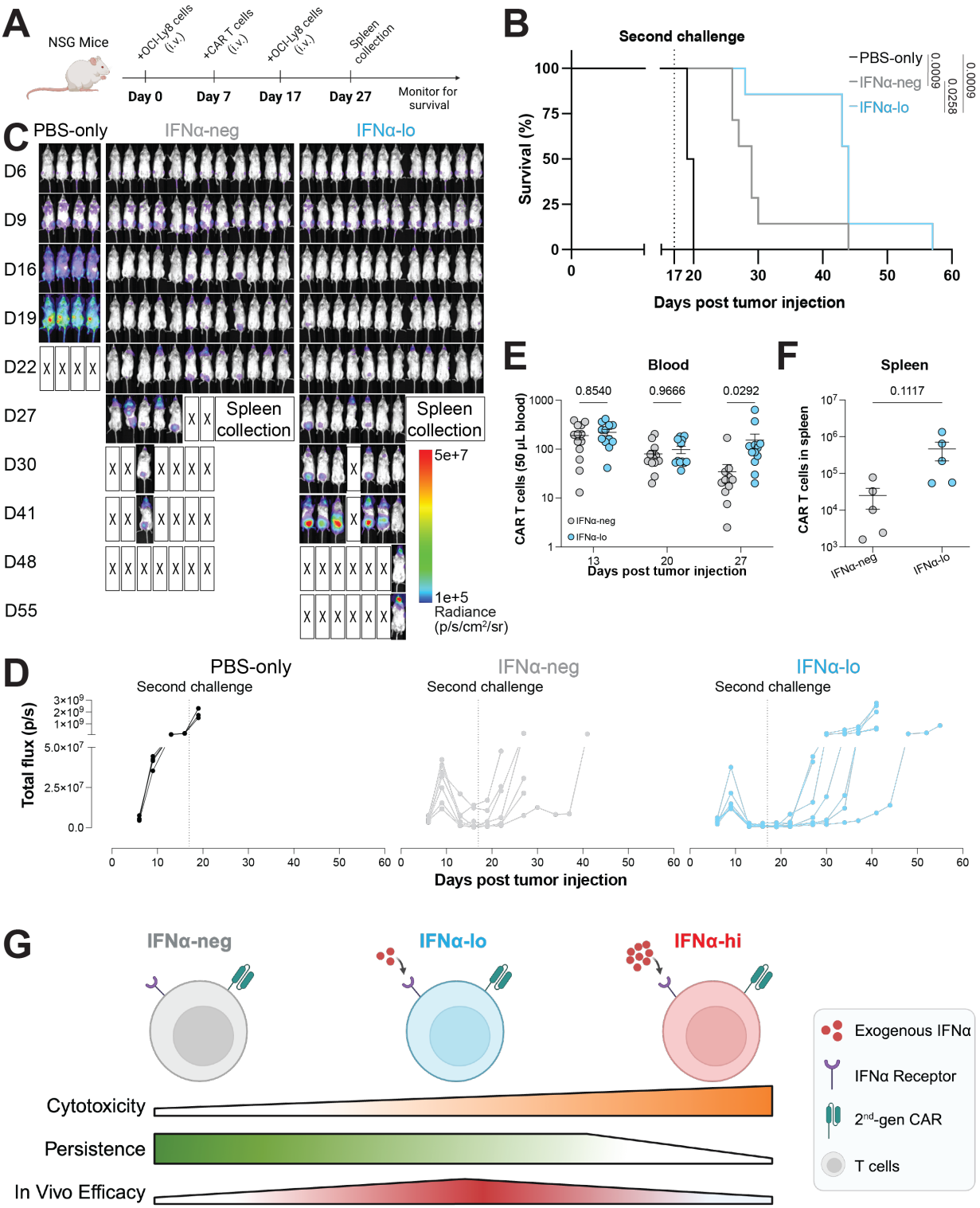

868